

# Shear-driven and diffusive helicity fluxes in $\alpha\Omega$ dynamos

G. Guerrero,<sup>1\*</sup> P. Chatterjee<sup>1</sup> and A. Brandenburg<sup>1,2</sup>

<sup>1</sup>*Nordita, AlbaNova University Center, Roslagstullsbacken 23, SE 10691 Stockholm, Sweden*

<sup>2</sup>*Department of Astronomy, AlbaNova University Center, Stockholm University, SE 10691 Stockholm, Sweden*

Accepted 2010 July 22. Received 2010 July 22; in original form 2010 May 26

## ABSTRACT

We present non-linear mean-field  $\alpha\Omega$  dynamo simulations in spherical geometry with simplified profiles of kinetic  $\alpha$  effect and shear. We take magnetic helicity evolution into account by solving a dynamical equation for the magnetic  $\alpha$  effect. This gives a consistent description of the quenching mechanism in mean-field dynamo models. The main goal of this work is to explore the effects of this quenching mechanism in solar-like geometry, and in particular to investigate the role of magnetic helicity fluxes, specifically diffusive and Vishniac–Cho (VC) fluxes, at large magnetic Reynolds numbers ( $R_m$ ). For models with negative radial shear or positive latitudinal shear, the magnetic  $\alpha$  effect has predominantly negative (positive) sign in the Northern (Southern) hemisphere. In the absence of fluxes, we find that the magnetic energy follows an  $R_m^{-1}$  dependence, as found in previous works. This catastrophic quenching is alleviated in models with diffusive magnetic helicity fluxes resulting in magnetic fields comparable to the equipartition value even for  $R_m = 10^7$ . On the other hand, models with a shear-driven Vishniac–Cho flux show an increase in the amplitude of the magnetic field with respect to models without fluxes, but only for  $R_m < 10^4$ . This is partly a consequence of assuming a vacuum outside the Sun which cannot support a significant VC flux across the boundary. However, in contrast to the diffusive flux, the VC flux modifies the distribution of the magnetic field. In addition, if an ill-determined scaling factor in the expression for the VC flux is large enough, subcritical dynamo action is possible that is driven by the action of shear and the divergence of magnetic helicity flux.

**Key words:** hydrodynamics – magnetic fields – MHD – turbulence.

## 1 INTRODUCTION

A crucial point in the study of astrophysical dynamos is to understand the mechanism by which they saturate. Nevertheless, a consistent description of this process has rarely been considered in mean-field dynamo (MFD) modelling and only a heuristic description is often used. An important phenomenon occurs when the dynamo operates in closed or periodic domains: the turbulent contribution to the dynamo equation, i.e. the  $\alpha$  effect, decreases for large values of the magnetic Reynolds number ( $\alpha \sim R_m^{-1}$ ). This process is known as catastrophic quenching and can pose a problem in explaining the generation of magnetic field in late-type stars like the Sun or in the Galaxy, where  $R_m$  could be of the order of  $10^9$  or  $10^{15}$ , respectively.

In the last few years the nature of the catastrophic quenching has been identified as a consequence of magnetic helicity conservation (for a review see Brandenburg & Subramanian 2005a). It has been found that in the non-linear phase of the dynamo process, the back-reaction of the magnetic field on the velocity, due to the Lorentz

force, gives rise to a magnetic  $\alpha$  effect ( $\alpha_M$ ) with a sign opposite to the inductive contribution due to the helical motions, i.e. the kinetic  $\alpha$  effect. As the production of  $\alpha_M$  depends on  $R_m$ , the final value of the magnetic field should follow the same dependence. However, real astrophysical bodies are not closed systems, but they have open boundaries that may allow a flux of magnetic helicity. The shedding of magnetic helicity may mitigate the catastrophic  $\alpha$  quenching.

These ideas have been tested in direct numerical simulations (DNS) in both local Cartesian and global spherical domains. In the former case (Brandenburg 2005; Käpylä, Korpi & Brandenburg 2008) it has been shown that open boundaries (e.g. vertical field boundary conditions) lead to a faster saturation of a large-scale magnetic field compared with cases in closed domains (perfect conductor or triple-periodic boundary conditions). In the latter, it has been found that it is possible to build up large-scale magnetic fields either with forced turbulence (Brandenburg 2005; Mitra et al. 2010b) or with convectively driven turbulence (e.g. Brown et al. 2010; Käpylä et al. 2010). These models generally used vertical field boundary conditions.

In flux-transport dynamos (Dikpati & Charbonneau 1999; Guerrero & de Gouveia Dal Pino 2008) as well as in interface dynamos of the solar cycle (e.g. Charbonneau & MacGregor 1997;

\*E-mail: guerrero@nordita.org

MacGregor & Charbonneau 1997) the quenching mechanism has been considered either through an *ad hoc* algebraic equation or by phenomenological considerations (Chatterjee, Nandy & Choudhuri 2004), but most of the time the models do not consider the effects of magnetic helicity conservation. An exception is the recent paper by Chatterjee, Brandenburg & Guerrero (2010a), where these effects have been considered in the context of an interface dynamo.

Magnetic helicity often evolves on slow time-scales, so it is necessary to solve an additional dynamical equation for the contribution of the small-scale field to the magnetic helicity together with the induction equation for the mean magnetic field. The latter equation implies the evolution of magnetic helicity from the large-scale field, so that contribution is automatically included. Magnetic helicity losses from large-scale fields have in principle an adverse effect on the saturation amplitude (Brandenburg, Dobler & Subramanian 2002). In fact the contributions from small-scale and large-scale fields can be equally big (Blackman & Brandenburg 2003). In the past few years, some effort has already been made to consider this dynamical saturation mechanism in MFD models like in the 1D  $\alpha^2$  dynamo models presented in Brandenburg, Candelaresi & Chatterjee (2009), in axisymmetric models in cylindrical geometry for the galactic  $\alpha\Omega$  dynamo (Shukurov et al. 2006; Sur, Shukurov & Subramanian 2007), and also in models with spherical geometry for an  $\alpha^2$  dynamo (Brandenburg et al. 2007). The role of various kinds of magnetic helicity fluxes has been explored in several papers (Shukurov et al. 2006; Zhang et al. 2006; Brandenburg et al. 2009). All these models show that catastrophic quenching can be alleviated even when the magnetic helicity fluxes from small-scale and large-scale fields are equally big.

Our ultimate goal is to develop a self-consistent MFD model of the Sun, with observed velocity profiles and turbulent dynamo coefficients computed from DNS. This is a task that requires intensive efforts. Hence we shall proceed step by step, starting with simple models and then including more realistic physics on the way. In this work we will study the effects of magnetic helicity conservation in simplified  $\alpha\Omega$  dynamo models for a considerable number of cases. More importantly, we shall perform our calculations in spherical geometry, which is appropriate for describing stellar dynamos, with suitable boundary conditions, and considering shear profiles that are a simplified version of the observed solar differential rotation. We shall also explore how magnetic helicity fluxes affect the properties of the solution. Two classes of fluxes are considered in this paper: a diffusive flux and a shear-driven or Vishniac–Cho (hereafter VC) flux (Vishniac & Cho 2001). We consider models with either radial or latitudinal shear. The effects of meridional circulation will be investigated in detail in a companion paper (Chatterjee, Guerrero & Brandenburg 2010b).

This paper is organized as follows: in Section 2 we describe the basic mathematical formalism of the  $\alpha\Omega$  dynamo, give the formulation of the equation for  $\alpha_M$  and also justify the fluxes included. In Section 3 we describe the numerical method and then, we present our results in Section 4 starting from a dynamo model with algebraic quenching to models with dynamical  $\alpha$  quenching and different fluxes. Finally, we provide a summary of this work in Section 5.

## 2 THE $\alpha\Omega$ DYNAMO MODEL

In mean-field dynamo theory, the evolution of the magnetic field is described by the mean-field induction equation,

$$\frac{\partial \bar{\mathbf{B}}}{\partial t} = \nabla \times (\bar{\mathbf{U}} \times \bar{\mathbf{B}} + \bar{\mathcal{E}} - \eta_m \nabla \times \bar{\mathbf{B}}), \quad (1)$$

where  $\bar{\mathbf{B}}$  and  $\bar{\mathbf{U}}$  represent the mean magnetic and velocity fields, respectively;  $\eta_m$  is the molecular diffusivity;  $\bar{\mathcal{E}} = \alpha \bar{\mathbf{B}} - \eta_t \mu_0 \bar{\mathbf{J}}$  is the mean electromotive force obtained under the assumption of homogeneity and isotropy using a closure theory like the first-order smoothing approximation (FOSA), where  $\bar{\mathcal{E}}$  gives the contribution of the small-scale components on the large-scale field;  $\alpha$  is the non-diffusive contribution of the turbulence;  $\eta_t$  is the turbulent magnetic diffusivity;  $\bar{\mathbf{J}} = \nabla \times \bar{\mathbf{B}} / \mu_0$  is the mean current density; and  $\mu_0$  is the vacuum permeability.

In spherical coordinates and under the assumption of axisymmetry, it is possible to split magnetic and velocity fields into their azimuthal and poloidal components,  $\bar{\mathbf{B}} = B \hat{\boldsymbol{\phi}} + \nabla \times (A \hat{\boldsymbol{\phi}})$  and  $\bar{\mathbf{U}} = r \sin \theta \Omega \hat{\boldsymbol{\phi}} + \bar{\mathbf{U}}_p$ , respectively. For the sake of simplicity we shall not consider the meridional component of the flow, i.e.  $\bar{\mathbf{U}}_p = 0$ . Then, the toroidal and poloidal components of equation (1) may be written as

$$\frac{\partial B}{\partial t} = s \mathbf{B}_p \cdot \nabla \Omega - [\nabla \eta \times (\nabla \times B \hat{\boldsymbol{\phi}})]_{\phi} + \eta D^2 B, \quad (2)$$

$$\frac{\partial A}{\partial t} = \alpha B + \eta D^2 A, \quad (3)$$

where  $D^2 = \nabla^2 - s^{-2}$  is the diffusion operator,  $\eta = \eta_m + \eta_t$ ,  $s = r \sin \theta$  is the distance from the axis and  $\mathbf{B}_p = \nabla \times (A \hat{\boldsymbol{\phi}})$  is the poloidal field.

The two source terms in equations (2) and (3),  $s \mathbf{B}_p \cdot \nabla \Omega$  and  $\alpha B$ , express the inductive effects of shear and turbulence, respectively. The relative importance of these two effects may be quantified through the non-dimensional dynamo numbers:  $C_\Omega = \Delta \Omega L^2 / \eta$  and  $C_\alpha = \alpha_0 L / \eta$ , where  $\Delta \Omega$  is the angular velocity different between top and bottom of the domain. Note that equations (2) and (3) are valid only in the limit  $C_\Omega \gg C_\alpha$ , known as  $\alpha\Omega$  dynamo.

The inductive effects of shear may be understood as the stretching of the magnetic field lines due to the change in the angular velocity between two adjacent points. On the other hand, the kinetic  $\alpha$ -effect is the consequence of helical motions of the plasma which produce screw-like motions in the rising blobs of the magnetic field. Using the first-order smoothing approximation in the high  $R_m$  limit, together with the assumption of isotropy, it may be expressed as

$$\alpha_K = -\frac{1}{3} \tau \overline{\boldsymbol{\omega} \cdot \mathbf{u}}, \quad (4)$$

where  $\tau$  is the correlation time of the turbulent motions and  $\boldsymbol{\omega} = \nabla \times \mathbf{u}$  is the small-scale vorticity. The saturation value of the magnetic field may be obtained by multiplying  $\alpha_K$  by the quenching function  $f_q = (1 + B^2 / B_{\text{eq}}^2)^{-1}$ , which stops the exponential growth of the magnetic field at values close to the equipartition field strength given by  $B_{\text{eq}} = (\mu_0 \rho \overline{u^2})^{1/2}$ . This form of algebraic quenching was introduced heuristically (see e.g. Stix 1972) and has often been used as the standard quenching mechanism in many dynamo simulations. However, it does not give information about the back-reaction process and is independent of any other parameter of the system like the magnetic Reynolds number. A consistent description of the quenching mechanism will be presented in the following section.

### 2.1 Dynamical $\alpha$ effect

It has been demonstrated that, when the amplitude of the magnetic field reaches values near the equipartition, the  $\alpha$ -effect is modified by a magnetic contribution, the so-called magnetic  $\alpha$  effect, denoted by  $\alpha_M$ . It is usually the case that  $\alpha_M$  has a sign opposite to  $\alpha_K$  resulting thus in the saturation of the magnetic field. Pouquet, Frisch

& Léorat (1976) have shown that  $\alpha_M$  is proportional to the small-scale current helicity of the system, hence it is possible to write  $\alpha$  as a sum of two contributions, one from the fluid turbulence and other from the magnetic field, as follows:

$$\alpha = \alpha_K + \alpha_M = -\frac{1}{3}\tau\overline{\boldsymbol{\omega} \cdot \mathbf{u}} + \frac{1}{3}\tau\overline{\mathbf{j} \cdot \mathbf{b}}/\bar{\rho}, \quad (5)$$

where  $\bar{\rho}$  is the mean density of the medium, assumed here as a constant, and  $\mathbf{j} = \nabla \times \mathbf{b}/\mu_0$  is the current density of the fluctuating field. In general  $\alpha_M$  is a tensor, but for the sake of simplicity we will assume here that it is a scalar. The mathematical expression that describes the evolution of  $\alpha_M$  may be obtained by taking into account the magnetic helicity evolution (Blackman & Brandenburg 2002), which leads to

$$\frac{\partial \alpha_M}{\partial t} = -2\eta_t k_f^2 \left( \frac{\overline{\boldsymbol{\mathcal{E}} \cdot \overline{\mathbf{B}}}}{B_{\text{eq}}^2} + \frac{\alpha_M}{R_m} \right) - \nabla \cdot \overline{\mathcal{F}}_\alpha, \quad (6)$$

where  $k_f = 2\pi/(L_0 - r_c)$  with  $r_c = 0.7L_0$  is a suitable choice for the wavenumber of the forcing scale; the magnetic Reynolds number is here defined as  $R_m = \eta_t/\eta_m$ ; and  $^1 \overline{\mathcal{F}}_\alpha$  is the flux of the magnetic  $\alpha$  effect related to the flux of the mean small-scale magnetic helicity,  $\overline{\mathbf{F}}_f$ , through

$$\overline{\mathcal{F}}_\alpha = \frac{\mu_0 \bar{\rho} \eta_t k_f^2}{B_{\text{eq}}^2} \overline{\mathbf{F}}_f. \quad (7)$$

According to previous authors  $\alpha_M$  has a large value in the interior of the domain in absence of fluxes ( $\overline{\mathcal{F}}_\alpha = 0$ ), and its sign is usually opposite to the sign of  $\alpha_K$  in such a way that the final amplitude of the total  $\alpha$ -effect decreases to a value close to the critical value for dynamo action. As a consequence, the final value of the magnetic energy decreases proportional to  $R_m^{-1}$ . An exception is the case with triply periodic boundaries where a super-equipartition field can be reached, albeit on a resistive time-scale (Brandenburg 2001).

## 2.2 Magnetic helicity fluxes

The mean-field magnetic helicity,  $\bar{h}$  has two contributions,  $\bar{h}_m = \overline{\mathbf{A} \cdot \overline{\mathbf{B}}}$ , corresponding to the helicity built by the large-scale magnetic fields, and  $\bar{h}_f = \overline{\mathbf{a} \cdot \mathbf{b}}$ , being the helicity due to the small-scale fields. The time evolution of  $\bar{h}_m$  depends on the evolution of the vectors  $\overline{\mathbf{B}}$  and  $\overline{\mathbf{A}}$ , which are obtained by solving equations (2) and (3). Then, the evolution of  $\bar{h}_m$  is implicitly considered in the system and its fluxes depend on the physics incorporated in the induction equation (in our case, for instance, shear and turbulent diffusion). On the other hand, the evolution of  $\bar{h}_f$  depends on both mean and fluctuating fields. We do not solve here the evolution equation for the small-scale magnetic fields, but instead we solve the equation for  $\alpha_M$  and capture with it the built-up of small-scale magnetic helicity in the system.

Recently it has been noticed that, although the saturation of the dynamo depends on the amount of magnetic helicity generated, catastrophic quenching is alleviated when there is a flux of small-scale magnetic helicity out of the domain, so that the total magnetic helicity inside need not be conserved any longer. We may introduce an ansatz (justified below) for these fluxes in the equation for  $\alpha_M$  using equation (7), which, in turn, is solved together with equations (2) and (3), giving a consistent evolution of the magnetic fields and the magnetic helicity.

<sup>1</sup> Note that with the FOSA result  $\eta_t = \tau u_{\text{rms}}^2/3 \approx u_{\text{rms}}/3k_f$  this definition of  $R_m$  implies  $R_m = u_{\text{rms}}/3\eta_m k_f$ .

Several contributions for the helicity flux have been derived in the past (Kleeorin & Rogachevskii 1999; Vishniac & Cho 2001; Subramanian & Brandenburg 2004). Amongst them are the flux of magnetic helicity across the isorotation surfaces, advective and diffusive fluxes and also the explicit removal of magnetic helicity in processes like solar coronal mass ejections or galactic fountain flows, for the case of the galactic dynamo (Shukurov et al. 2006).

From the mathematical point of view, the nature of the flux terms in the equation for  $\alpha_M$  has not been demonstrated with sufficient rigor. However, several DNS have pointed to their existence. First, the shearing box convection simulations of Käpylä et al. (2008) showed that in the presence of open boundaries, the large-scale magnetic field grows on temporal scales much shorter than the dissipative time-scale. They concluded from this that open boundaries may allow the magnetic helicity to escape out of the system. These experiments seem to be compatible with the helicity flux proposed by Vishniac & Cho (2001), whose functional form may be expressed as (see Subramanian & Brandenburg 2004; Brandenburg & Subramanian 2005b, for further details and underlying assumptions):

$$\overline{\mathbf{F}}_i^{\text{VC}} = C_{\text{VC}} \epsilon_{ijkl} \overline{\mathbf{S}}_{lk} \overline{B}_j \overline{B}_k, \quad (8)$$

where  $\overline{\mathbf{S}}_{lk} = \frac{1}{2}(\overline{U}_{l,k} + \overline{U}_{k,l})$  is the mean rate of strain tensor and  $C_{\text{VC}}$  is a non-dimensional scaling factor. As we assume  $\mathbf{U}_p = 0$ , this flux has the following three components:

$$\overline{\mathbf{F}}_r^{\text{VC}} = C_{\text{VC}} [\overline{\mathbf{S}}_{\phi r} B_\theta B_r + \overline{\mathbf{S}}_{\theta \phi} (B_\theta^2 - B_\phi^2)], \quad (9)$$

$$\overline{\mathbf{F}}_\theta^{\text{VC}} = C_{\text{VC}} [-\overline{\mathbf{S}}_{\phi \theta} B_r B_\theta + \overline{\mathbf{S}}_{r\phi} (B_\phi^2 - B_r^2)], \quad (10)$$

$$\overline{\mathbf{F}}_\phi^{\text{VC}} = C_{\text{VC}} [\overline{\mathbf{S}}_{\theta \phi} B_r B_\phi - \overline{\mathbf{S}}_{r\phi} (B_\theta^2 - B_\phi^2)], \quad (11)$$

with  $\overline{\mathbf{S}}_{\phi r} = \overline{\mathbf{S}}_{r\phi} = \frac{1}{2} r \sin \theta \partial \Omega / \partial r$  and  $\overline{\mathbf{S}}_{\theta \phi} = \overline{\mathbf{S}}_{\phi \theta} = \frac{1}{2} \sin \theta \partial \Omega / \partial \theta$ .

Secondly, Mitra et al. (2010a) performed  $\alpha^2$  dynamo simulations driven by forced turbulence in a box with kinetic helicity changing sign about the equator. They found that the diffusive flux of  $\alpha_M$  across the equator can be fitted to a Fickian diffusion law given by

$$\overline{\mathcal{F}}_D = -\kappa_\alpha(r) \nabla \alpha_M. \quad (12)$$

They also computed the numerical value of this diffusion coefficient, and found it to be of the order of the turbulent diffusion coefficient. They also found that the time-averaged flux is gauge independent. Both results were later corroborated by simulations without equator and instead a prescribed decline of kinetic helicity toward the boundaries (Hubbard & Brandenburg 2010a).

Additionally, magnetic helicity may be advected by a mean velocity with a flux given by  $\overline{\mathcal{F}}_{\text{ad}} = \alpha_M \overline{\mathbf{U}}$  and expelled from stellar interiors by coronal mass ejections (CMEs), by stellar wind or by galactic fountain flows if applied to the galactic dynamo (Shukurov et al. 2006; Sur et al. 2007). In the Sun this advective flux,  $\mathcal{F}_{\text{CME}}$ , may account for  $\sim 10$  per cent of the total helicity generated by the solar differential rotation, as estimated by Berger & Ruzmaikin (2000). It can be modelled by artificially removing a small amount of  $\alpha_M$  every  $\tau$  time (Brandenburg et al. 2009), or also by a radial velocity field that mimics the solar wind.

The total flux of magnetic helicity may be written as the sum of these contributions,

$$\overline{\mathcal{F}} = \overline{\mathcal{F}}_{\text{VC}} + \overline{\mathcal{F}}_D + \overline{\mathcal{F}}_{\text{ad}} + \overline{\mathcal{F}}_{\text{CME}}. \quad (13)$$

Since in our dynamo model we do not include any component of the velocity field other than the differential rotation, we will consider only the first two terms on the right-hand side of equation (13).

In general, fluxes of large-scale magnetic helicity are also present, but they would only be of diagnostic and not of prognostic use. Furthermore, such fluxes are cumbersome to evaluate, because only a gauge-independent computation is physically meaningful.

### 3 THE MODEL

We solve equations (2), (3) and (6) for  $A$ ,  $B$  and  $\alpha_M$  in the meridional plane in the range  $0.6L_0 \leq r \leq L_0$  and  $0 \leq \theta \leq \pi$ . We consider two different layers inside the spherical shell. In the inner one the dynamo production terms are zero and go smoothly to a finite value in the external layer. The magnetic diffusivity changes from a molecular to a turbulent value from the bottom to the top of the domain. This is achieved by considering error function profiles for the magnetic diffusivity, the differential rotation and the kinetic  $\alpha$  effect, respectively (see Fig. 1):

$$\eta(r) = \eta_m + \eta_t \Theta(r, r_1, w_1), \quad (14)$$

$$\frac{\partial \Omega}{\partial r}(r) = C_\Omega \left( \frac{\eta_t}{L_0^3} \right) \Theta(r, r_2, w_1), \quad (15)$$

$$\alpha_K(r, \theta) = C_\alpha \left( \frac{\eta_t}{L_0} \right) \Theta(r, r_1, w_1) \cos \theta, \quad (16)$$

where  $\Theta(r, r_{1,2}, w) = \frac{1}{2} \{1 + \text{erf}[(r - r_{1,2})/w]\}$ , with  $r_1 = 0.7L_0$ ,  $r_2 = 0.72L_0$  and  $w_1 = 0.025L_0$ . We fix  $C_\Omega = -10^4$  and vary  $C_\alpha$ .

The boundary conditions are chosen as follows: at the poles,  $\theta = 0, \pi$ , we impose  $A = B = 0$ ; at the base of the domain, we impose a perfect conductor boundary condition, i.e.  $A = \partial(rB)/\partial r = 0$ .

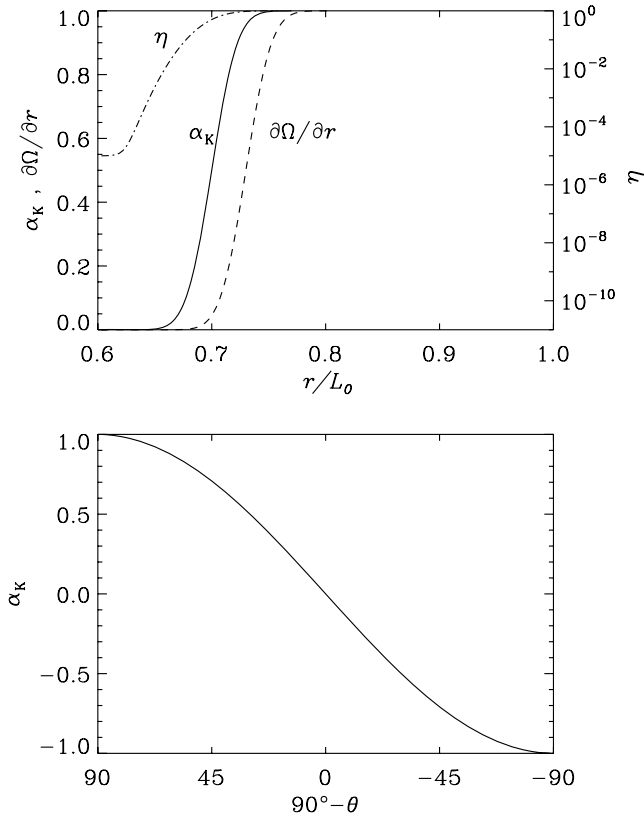


**Figure 1.** Profiles of the dynamo ingredients,  $\alpha_K$  (solid line),  $\partial\Omega/\partial r$  (dashed line) and  $\eta_t$  (dot-dashed line). All quantities are normalized to their maximum value.

Unless noted otherwise, we use at the top a vacuum condition by coupling the magnetic field inside with an external potential field (PF), i.e.  $(\nabla^2 - s^{-2})A = 0$ . A good description of the numerical implementation of this boundary condition may be found in Dikpati & Choudhuri (1994).

The equations for  $A$  and  $B$  are solved using a second-order Lax–Wendroff scheme for the first derivatives, and centred finite differences for the second-order derivatives. The temporal evolution is computed by using a modified version of the ADI method of Peaceman & Rachford (1955) as explained in Dikpati & Charbonneau (1999). This numerical scheme has been used previously in several works on the flux-transport dynamo and the results were found to be in good agreement with those using other numerical techniques (Guerrero & de Gouveia Dal Pino 2007, 2008; Guerrero et al. 2009).

In the absence of magnetic helicity fluxes, equation (6) for  $\alpha_M$  corresponds to an initial value problem that can be solved explicitly. However, as we are going to include a diffusive flux, we use for  $\alpha_M$  the same numerical technique used for  $A$  and  $B$  and in this case we consider  $\alpha_M = 0$  on all boundaries. All the source terms on the right-hand side of equation (6) are computed explicitly. When considering magnetic helicity and its fluxes, one must worry about the gauge dependence of the solutions. Here we invoke the idea of scale separation, in particular, Subramanian & Brandenburg (2006) have shown that it is possible to write a gauge-independent equation for the local magnetic helicity density. Their expressions correspond to our equation (6).

Furthermore, we have tested the convergence of the solution for  $64^2$ ,  $128^2$  and  $256^2$  grid points. For cases with small  $R_m$ , there are no significant differences between different resolutions, but for high  $R_m$ ,  $64^2$  grid points is insufficient to properly resolve the sharp diffusivity gradient. A resolution of  $128^2$  grid points is a good compromise between accuracy and speed.

## 4 RESULTS

### 4.1 $\alpha\Omega$ dynamos with algebraic quenching

In order to characterize our  $\alpha\Omega$  dynamo model we start by exploring the properties of the system when the saturation is controlled by algebraic quenching with  $f_q = (1 + B^2/B_{\text{eq}}^2)^{-1}$ . We find that, with the profiles given by equations (14)–(16), Fig. 1, the critical dynamo number is around  $-2 \times 10^4$  (i.e.  $C_\alpha^c = 1.975$ ). The solution for the model is a dynamo wave traveling towards the equator since it obeys the Parker (1955)–Yoshimura (1975) sign rule (see Fig. 2). In this

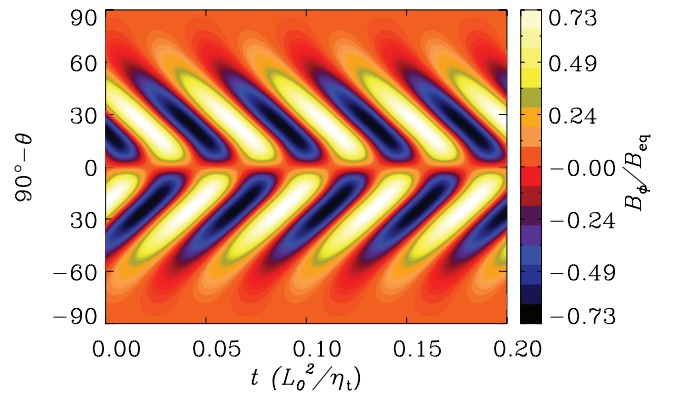


**Figure 2.** Time–latitude butterfly diagram for the toroidal component of the magnetic field at  $r = 0.72L_0$ , for an  $\alpha\Omega$  dynamo model with  $C_\Omega = -10^4$  and  $C_\alpha = 2.5$  and algebraic quenching.

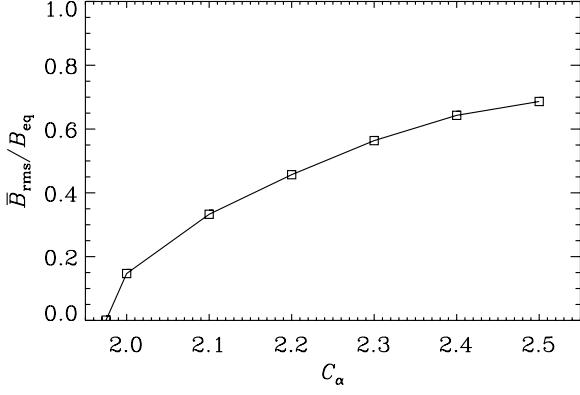


**Figure 3.** Magnetic field strength averaged over volume and time as a function of  $C_\alpha$  using an algebraic quenching function that is independent of  $R_m$ .

case, the saturated value of the magnetic field strength depends only on the dynamo number of the system,  $C_\alpha C_\Omega$ , as can be seen in the bifurcation diagram in Fig. 3. The quenching formula is here independent of  $R_m$ , so the saturation amplitude is also independent on  $R_m$ .

#### 4.2 Dynamical quenching with $\bar{\mathcal{F}}_\alpha = 0$

In this section we consider dynamo saturation through the dynamical equation for  $\alpha_M$  described in Section 2.1. In this models we distinguish three different stages in the time evolution of the magnetic field: a linear growth phase, a saturation phase and a final relaxation stage (see Fig. 4 and panels a–c of Fig. 5). The magnetic field is amplified from its initial value,  $5 \times 10^{-4} B_{eq}$ , following an exponential growth. From the earliest stages of the evolution we notice the growth of  $\alpha_M$  with values that are predominantly negative in the Northern hemisphere and positive in the Southern hemisphere. The latitudinal distribution of  $\alpha_M$  is fairly uniform in the active dynamo region, spanning from the equator to  $\sim \pm 60^\circ$  latitude. The radial distribution exhibits two narrow layers where the sign of  $\alpha_M$  is opposite to its dominant one developing at each hemisphere. These are located at the base of the dynamo region ( $r \sim 0.7L_0$ ) and near the surface ( $r > 0.95$ ). In the equation for the magnetic  $\alpha$  effect, equation (6), the production term is proportional to  $\bar{\mathcal{E}} \cdot \bar{\mathbf{B}} = \alpha \bar{\mathbf{B}}^2 - \eta_t \mu_0 \bar{\mathbf{J}} \cdot \bar{\mathbf{B}}$ . Since the value of  $\alpha_K$  is larger than

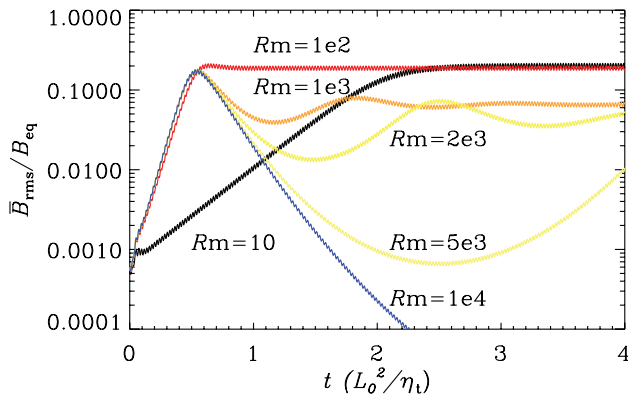


**Figure 4.** Time evolution of the averaged mean magnetic field for different values of  $R_m$ . No helicity fluxes have been considered for these models. Note that for  $R_m > 10^3$ , we have allowed the simulations to evolve for more than four diffusion times, as indicated in Table 1.

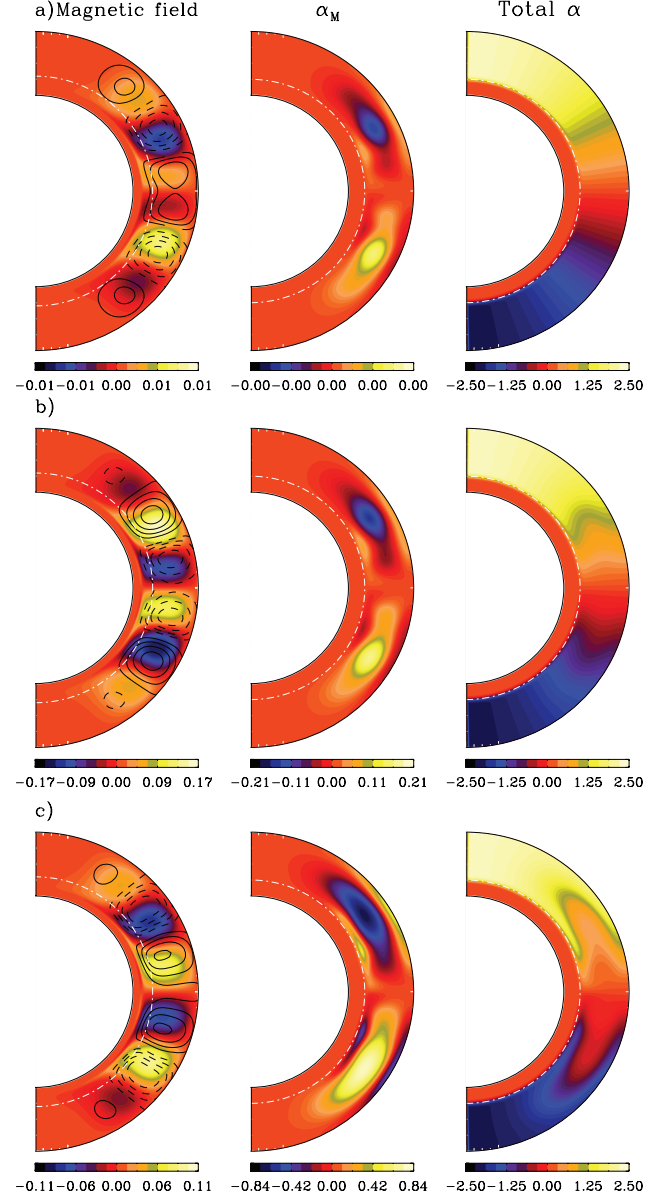


**Figure 5.** Meridional snapshots of three different phases of evolution of the dynamo model with dynamical quenching, (a)  $t = 0.25 (L_0^2/\eta_t)$ , (b)  $t = 0.5 (L_0^2/\eta_t)$  and (c)  $t = 2.0 (L_0^2/\eta_t)$ . The left-hand panels show the contours of toroidal magnetic field in colour scale, and clockwise (anticlockwise) poloidal magnetic field lines are shown in solid (dashed) lines. The central panels show the distribution of  $\alpha_M$ , and the right-hand panel shows the distribution of the total  $\alpha$ . All values are in non-dimensional units (i.e.  $B/B_{eq}$ ), so that the colour scale is different for each figure as indicated in colour bars.

the value of  $\alpha_M$  in the bulk of the domain, the first component of this term has the same sign as  $\alpha_K$ , which in general is positive in the northern and negative in the southern part of the domain. The minus sign in front of the right-hand side of equation (6) defines then the sign of  $\alpha_M$ . However, at the base and at the top of the dynamo region,  $\alpha_K \rightarrow 0$  and  $B \rightarrow 0$ , respectively. The term  $\eta_t \bar{\mathbf{J}} \cdot \bar{\mathbf{B}}$  is here the only source of  $\alpha_M$  and leads to the formation of these two thin layers.

In Fig. 5 we present the meridional distribution of the magnetic field (left-hand panel),  $\alpha_M$  (middle panel) and the total  $\alpha$  (right-hand panel), in normalized units, for the three different stages of

**Table 1.** Summary of main parameters and results of the numerical simulations.  $\overline{B}_{\text{rms}}$  is the value of the magnetic field averaged over volume and time,  $T$  is the dynamo cycle period. For all the simulations  $C_{\Omega} = -10^4$  except for the last five entries (with subscript  $\theta$ ) where  $C_{\Omega} = 5 \times 10^4$ .

Run	$C_{\alpha}$	$R_m$	$\kappa_{\alpha}(\eta_t)$	$C_{\text{VC}}$	$\overline{B}_{\text{rms}}/B_{\text{eq}}$	$T (L_0^2/\eta_t)$	$t (L_0^2/\eta_t)$
Ca <sup>C</sup>	1.975	10	-	-	0.0008	0.0486	1.0
Ca2.0	2.0	10	-	-	0.15	0.0484	1.0
Ca2.1	2.1	10	-	-	0.33	0.0477	3.0
Ca2.2	2.2	10	-	-	0.45	0.0471	3.0
Ca2.3	2.3	10	-	-	0.56	0.0464	3.0
Ca2.4	2.4	10	-	-	0.64	0.0460	3.0
Ca2.5	2.5	10	-	-	0.69	0.0455	3.0
Rm10	2.5	10	-	-	0.21	0.0422	4.0
Rm50	2.5	50	-	-	0.25	0.0446	4.0
Rm1e2	2.5	100	-	-	0.2	0.0455	4.0
Rm1e3	2.5	10 <sup>3</sup>	-	-	0.07	0.0464	4.0
Rm2e3	2.5	2 × 10 <sup>3</sup>	-	-	0.05	0.0464	6.0
Rm5e3	2.5	5 × 10 <sup>3</sup>	-	-	0.03	0.0468	15.0
Rm1e4	2.5	10 <sup>4</sup>	-	-	0.02	0.048	15.0
DRm10	2.5	10	0.005	-	0.22	0.0422	4.0
DRm50	2.5	50	0.005	-	0.26	0.0446	4.0
DRm1e2	2.5	100	0.005	-	0.20	0.0455	4.0
DRm1e3	2.5	10 <sup>3</sup>	0.005	-	0.09	0.0460	4.0
DRm1e4	2.5	10 <sup>4</sup>	0.005	-	0.06	0.0457	5.0
DRm1e5	2.5	10 <sup>5</sup>	0.005	-	0.05	0.0460	7.0
DRm1e6	2.5	10 <sup>6</sup>	0.005	-	0.05	0.0457	8.0
DRm1e7a	2.5	10 <sup>7</sup>	0.001	-	0.026	0.0457	20.0
DRm1e7b	2.5	10 <sup>7</sup>	0.005	-	0.05	0.0460	10.0
DRm1e7c	2.5	10 <sup>7</sup>	0.01	-	0.073	0.0460	10.0
DRm1e7d	2.5	10 <sup>7</sup>	0.03	-	0.12	0.0460	8.0
DRm1e7e	2.5	10 <sup>7</sup>	0.05	-	0.15	0.0457	4.0
DRm1e7f	2.5	10 <sup>7</sup>	0.1	-	0.20	0.0460	4.0
DRm1e7g	2.5	10 <sup>7</sup>	1.0	-	0.54	0.0458	4.0
DRm1e7h	2.5	10 <sup>7</sup>	5.0	-	1.23	0.060	4.0
DRm1e7i	2.5	10 <sup>7</sup>	10.0	-	1.76	0.0457	4.0
VCa	2.5	10 <sup>3</sup>	-	0.002	0.032	0.0449	4.0
VCb	2.5	10 <sup>3</sup>	-	0.01	0.02	0.0442	4.0
VCc	2.5	10 <sup>3</sup>	-	-0.002	0.02	0.0447	4.0
VCD	2.5	10 <sup>4</sup>	-	-0.002	-	-	4.0
VCD	2.5	10 <sup>3</sup>	0.1	0.001	0.11	0.0446	4.0
Re1e3 <sub>θ</sub>	2.5	10 <sup>3</sup>	-	-	0.023	0.0282	8.0
VC <sub>θ</sub> a	2.5	10 <sup>3</sup>	-	0.004	0.04	0.033	4.0
VCD <sub>θ</sub>	2.5	10 <sup>3</sup>	0.1	0.004	0.062	0.0266	4.0
Re1e3 <sub>θ</sub> vf	2.5	10 <sup>3</sup>	-	-	0.036	0.032	6.0
VC <sub>θ</sub> vf	2.5	10 <sup>3</sup>	-	0.004	0.075	0.033	6.0

evolution corresponding to the early kinematic phase, the late kinematic phase and the saturated phase. These snapshots correspond to the simulation with  $R_m = 10^3$  (Run Rm1e3 in Table 1).

The morphology of toroidal magnetic field, represented by filled contours, corresponds to a multilobed pattern of alternating polarity (left-hand panels of Fig. 5). These lobes are uniformly distributed in radius in the whole dynamo region with maximum amplitude at the base of this layer. The poloidal magnetic field, shown by continuous (clockwise) and dashed (anticlockwise) streamlines, follows a similar pattern with lines that are open at the top of the domain due to the PF boundary condition. This multilobed pattern remains unchanged during the evolution even though its amplitude changes. There is a phase shift between toroidal and poloidal components which we have estimated to be  $\sim 0.4\pi$ . The model preserves the initial dipolar parity during the entire evolution.

The magnetic  $\alpha$  effect (middle panels) is formed first at latitudes between  $\pm 30^\circ$  and then it amplifies and expands to latitudes up to

$\sim \pm 60^\circ$ . This makes the total  $\alpha$  effect, initially similar to  $\alpha_K$  (Fig. 1 and top panel of Fig. 5a), smaller at lower latitudes in the central area of the dynamo region. At the bottom and at the top of the domain  $\alpha_M$  and  $\alpha_K$  have the same sign, making the total  $\alpha$  larger. However, the global effect is a decrease of the dynamo efficiency.

The space–time evolution of  $\alpha_M$  depends on the value of the magnetic Reynolds number. For small  $R_m$ , the decay term in equation (6) (i.e. the second term in the parenthesis) becomes important, so that there is a competition between the production and decay terms resulting in an oscillatory behaviour in the amplitude of the magnetic  $\alpha$  effect. The period of these oscillations is half the period of the magnetic cycle. With increasing  $R_m$ , the amplitude of the oscillations decreases such that for  $R_m \leq 10^3$ ,  $\alpha_M$  is almost steady.

The evolution of  $\alpha_M$  traces the growth of the magnetic field, but its final value depends on the magnetic Reynolds number. For small  $R_m$ ,  $\alpha_M$  reaches a steady state after saturation, but for large  $R_m$ , its relaxation is modulated by damped oscillations. The relaxation time

is proportional to  $R_m$ , which means that for  $R_m \gg 1$  the simulation must run for many diffusion time units. The differences in the relaxation time observed for  $\alpha_M$  reflects the evolution of the magnetic field, as is shown in Fig. 4.

We observe that the rms value of the magnetic field remains steady during the saturation phase for  $R_m < 10^2$ . For  $10^2 < R_m < 10^3$ , a bump appears in the curve of magnetic field evolution, followed by the relaxation to a steady value, whereas for  $R_m > 10^3$ , the magnetic energy shows damped relaxations with a final energy proportional to  $R_m^{-1}$  as has been previously reported (Brandenburg et al. 2007). These oscillations in the time evolution of the averaged magnetic field have been reported in mean-field dynamo simulations including the dynamical  $\alpha$ -effect (Brandenburg & Subramanian 2005b).

Not many DNS of  $\alpha\Omega$  dynamos exist so far in the literature with  $R_m \geq 100$  that could be compared with our results. However, in the local  $\alpha\Omega$  dynamo simulations of Käpylä et al. (2008), a rapid decay of the magnetic field seems to occur after the initial saturation for moderate values of  $R_m$  ( $\leq 250$ ). This decay forms a bump in the curve of the averaged magnetic field (see their fig. 14), similar to the bump that we obtain for  $10^2 < R_m < 10^3$ . A similar bump is also seen in simulations with forced turbulence (Hubbard & Brandenburg 2010a).

For reasons of clarity in Fig. 4 we do not show the entire time evolution of each simulation with  $R_m > 10^3$ . The total evolution time as well as the final value of the magnetic field of each simulation are shown in Table 1. For magnetic Reynolds numbers above  $2 \times 10^4$ , the initial kinematic phase is followed by a decay phase during which the total  $\alpha$  effect goes through subcritical values and then the dynamo fails to start again.

One may think that, as the magnetic field is decaying to very small values, the value of  $\alpha_M$  should also be small, so that the magnetic field would not be quenched any longer. However, the decay rate of  $\alpha_M$  varies as  $R_m^{-1}$  (equation 6) which makes this quantity have a long memory that makes the recovery of the mean magnetic field from very low values occur only after several turbulent diffusion times.

### 4.3 Diffusive flux for $\alpha_M$ ( $\mathcal{F}_\alpha = \mathcal{F}_D$ )

In this section we consider the Fickian diffusion term in equation (12) for  $\alpha_M$ . We consider a diffusion coefficient,  $\kappa_\alpha$ , varying from  $5 \times 10^{-3}\eta_t$  to  $10\eta_t$  in the dynamo region and with  $\kappa_\alpha = \eta_m$  in the bottom layer. In these cases, the initial evolution of  $\alpha_M$  is similar to the cases presented in the previous section: negative (positive) values for  $\alpha_M$  in the Northern (Southern) hemisphere, with narrow regions of opposite values near the regions where  $\alpha_K = 0$  or  $B = 0$ . However, at the later stages,  $\alpha_M$  is much more diffuse in the entire domain and has only one sign in each hemisphere. This is the result of a cancellation of  $\alpha_M$  with opposite signs occurring in each hemisphere due to radial diffusion. Contrary to the cases without fluxes, we now obtain finite values of  $B_{\text{sat}}$  for large values of  $R_m$ , as can be seen in Fig. 6. All the cases depicted in this figure correspond to  $\kappa_\alpha = 0.005\eta_t$ . We notice that the final value of the magnetic field still remains small compared to the equipartition ( $\leq 0.1B_{\text{eq}}$ ), but it is clear that even this very modest diffusion prevents the  $\alpha$  effect from being catastrophically quenched. This is also evident from the top panel of Fig. 7, where we plot the final strength of  $\bar{B}$  as a function of  $R_m$ , for the cases with and without diffusive flux. In the middle and bottom panels of Fig. 7 we compare the behaviour of the normalized  $\alpha_M$ , at a given point inside the dynamo region, and also the cycle period,  $T$ , of the dynamo for models with and without

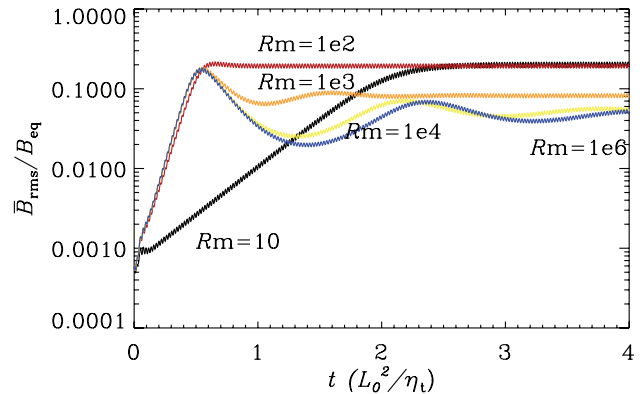


**Figure 6.** Same as Fig. 4 but for simulations including a diffusive flux of  $\alpha_M$ . All the simulations correspond to  $\kappa_\alpha = 0.005\eta_t$ . Note that the dynamo solutions are oscillatory. However, the oscillations have small amplitude and are almost invisible from the plot.

fluxes. In both panels it is clear that for  $R_m$  above  $\sim 10^3$ ,  $\alpha_M$  and  $T$  reach a saturated value.

Besides its dependence on  $R_m$ , the evolution of  $\alpha_M$  depends also on  $\kappa_\alpha$ . For models with  $\kappa_\alpha \ll \eta_t$ , the evolution of  $\alpha_M$  relies on  $R_m$ , but for  $\kappa_\alpha \geq 0.1\eta_t$ , the dissipation time of  $\alpha_M$  becomes comparable to, or even shorter, than the period of the dynamo cycle. This results in  $\alpha_M$  becoming oscillatory, as shown in the bottom panel of Fig. 8. The amplitude and the period of these oscillations depend on the value of  $\kappa_\alpha$ .

In the top panel of Fig. 8 we show the final value of the averaged mean magnetic field as a function of  $\kappa_\alpha$ . We observe that for  $\kappa_\alpha$  in the range  $(0.1-1)\eta_t$ , the value of  $\bar{B}_{\text{rms}}$  remains between 20 and 60 per cent of the equipartition, a value similar to the one obtained in the simulations using algebraic  $\alpha$  quenching (Section 4.1, Fig. 3). For  $\kappa_\alpha > \eta_t$ , superequipartition values of the magnetic field may be reached. This is because larger values of  $\kappa_\alpha$  result in oscillations of  $\alpha_M$  with larger amplitude, such  $\alpha_M$  may locally change its sign, increasing the value of the total  $\alpha$  in each hemisphere and thereby enhancing the dynamo action. Such high values of the diffusion of the magnetic helicity are unlikely in nature. The meridional distribution of the variables for a model with  $\kappa_\alpha = \eta_t$  is shown in Fig. 9

### 4.4 The Vishniac–Cho flux

Our next step is to explore the magnetic helicity flux proposed by Vishniac & Cho (2001) in the form given by equation (8). For the moment we set  $\kappa_\alpha = 0$ . In a previous study on the effects of the VC flux in a MFD model in Cartesian coordinates, Brandenburg & Subramanian (2005b) found that there exists a critical value for the parameter  $C_{\text{VC}}$  above which there is a runaway growth of the magnetic field that can only be stopped using an additional algebraic quenching similar to the one used in Section 4.1 applied now to the total  $\alpha$ . They found that this critical value,  $C_{\text{VC}*}$ , diminishes upon increasing the amount of shear. Since we have used a strong shear ( $C_\Omega = -10^4$ ) we use nominal values of  $C_{\text{VC}} = 10^{-3}$ , but without any algebraic quenching.

The term  $\nabla \cdot \mathcal{F}_{\text{VC}}$  develops a multilobed pattern which travels in the same direction as the dynamo wave, confirming that the VC flux follows the surfaces of isorotation. From equation (8), we see that the VC flux is proportional to the magnetic energy density. In the present case, with  $|C_\Omega| \gg |C_\alpha|$ , the spatial distribution of  $\nabla \cdot \mathcal{F}_{\text{VC}}/B_{\text{eq}}^2$  is dominated by the terms involving  $B_\phi^2$  in equations

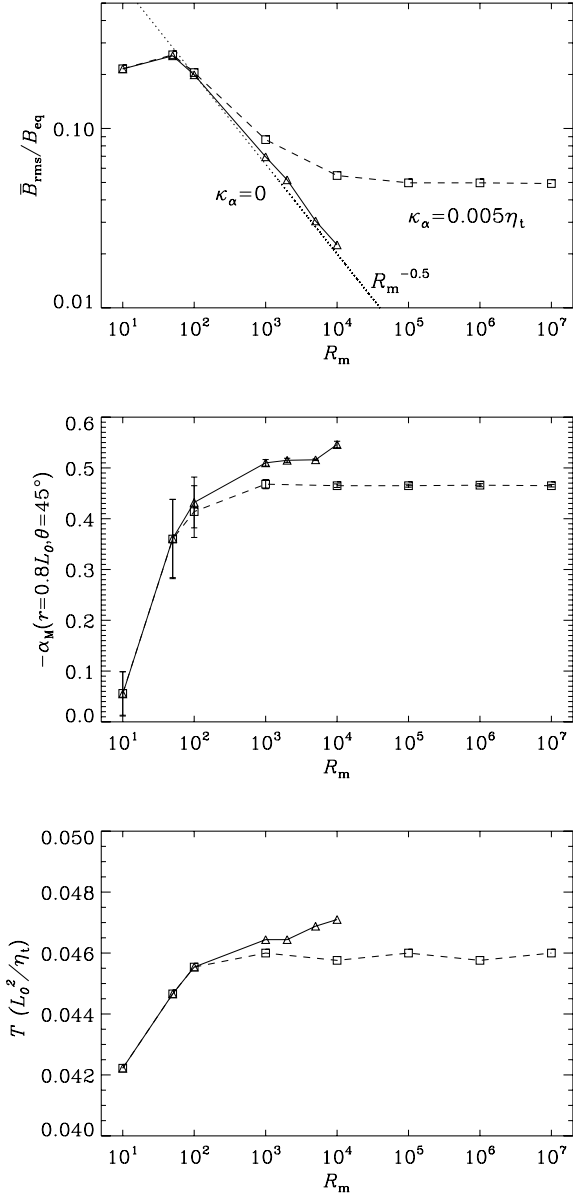


**Figure 7.**  $R_m$  dependence of the averaged mean magnetic field (top), the temporal mean value of  $\alpha_M$  at  $r = 0.8L_0$ ,  $\theta = 45^\circ$  (middle) and the dynamo cycle period,  $T$  in diffusion time units (bottom). The continuous lines present the result for simulations without diffusive flux of  $\alpha_M$  ( $\kappa_\alpha = 0$ ) and the dashed lines show the results for  $\kappa_\alpha = 0.005\eta_t$ . The error bars in the middle panel indicate the maximum and minimum values in the oscillations of  $\alpha_M$  at that point.

(9)–(11) (this may be inferred from the two left-hand panels of Fig. 10a). This results in a new distribution of  $\alpha_M$ , with concentrated regions of positive (negative) sign at low latitudes in the Northern (Southern) hemisphere, and a broad region of negative (positive) sign in latitudes between  $20^\circ$  and  $60^\circ$  (see middle panels of Fig. 10). Surprisingly we find that the general effect of this flux is to decrease the final amplitude of the magnetic field with respect to the case without any fluxes as can be seen in Fig. 11. Note that we have until now used only the potential field boundary condition for the poloidal field. When we consider both diffusive as well as VC fluxes, with  $\kappa_\alpha = 0.1\eta_t$  and  $C_{\text{VC}} = 10^{-3}$ , we obtain a magnetic field of slightly larger amplitude compared to the case with only the diffusive flux (compare the value of  $\bar{B}_{\text{rms}}$  in Runs DRm1e3 and VCD in Table 1).

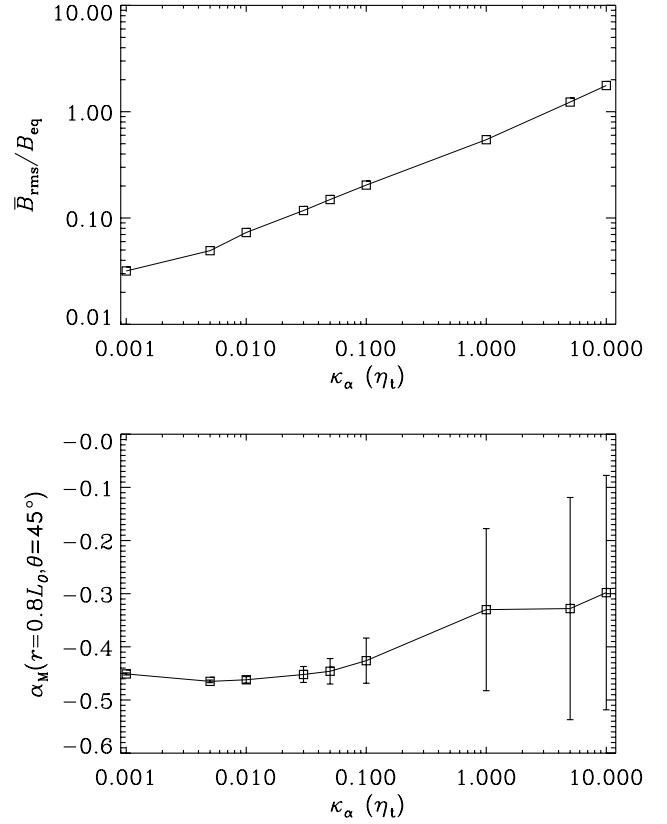


**Figure 8.** Top: final amplitude of the rms mean magnetic field for different values of  $\kappa_\alpha$  and  $R_m = 10^7$ . Bottom: final amplitude of  $\alpha_M$  at  $r = 0.8L_0$  and  $\theta = 45^\circ$ . The error bars indicate the maximum and minimum values in the oscillations of  $\alpha_M$  at this point.

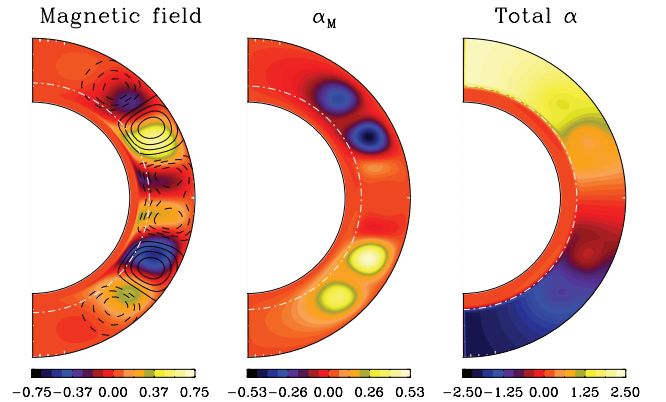


**Figure 9.** The same as Fig. 5 but for a diffusive flux with  $\kappa = \eta$ . The snapshot corresponds to  $t = 3.0$  ( $L_0/\eta_t$ ).

However, we may say from the butterfly diagram of Fig. 12 that the toroidal magnetic field appears to be more concentrated at lower latitudes, where the sign of  $\alpha_M$  is the same as that of  $\alpha_K$ .

With negative values of  $C_{\text{VC}}$ , it was found that the resulting profile of  $\alpha_M$  is only weakly modified from cases without fluxes, though its value is reduced marginally such that the final amplitude of  $\bar{B}_{\text{rms}}$  is slightly larger. But even this contribution does not help in alleviating catastrophic quenching in models with large  $R_m$  (see Fig. 11).

Since VC fluxes transport helicity along surfaces of constant shear, it may be expected that they are more important in models with latitudinal shear, since in this case the magnetic helicity

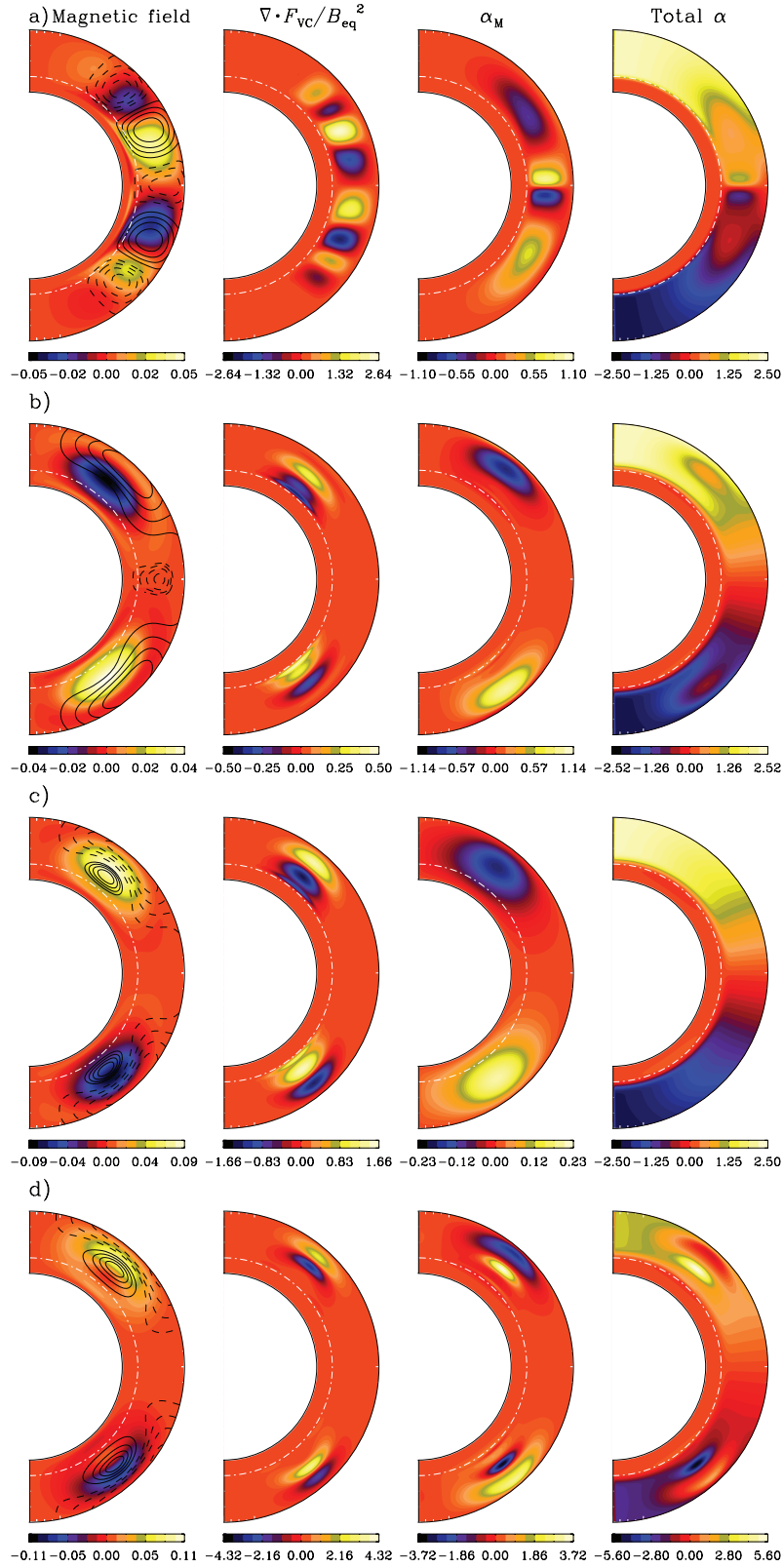


**Figure 10.** Meridional snapshots of the different models in Table 1: (a) VCa, (b)  $VC_{\theta}a$ , (c)  $VCD_{\theta}$  and (d)  $VC_{\theta}vf$ . The contours (colours and lines) for the magnetic field have the same meaning as in Fig. 5. In this plot we have included a new column with the value of the divergence of the VC flux term in the  $\alpha_M$  equation, i.e.  $\nabla \cdot \overline{\mathcal{F}}_{VC} / B_{eq}^2$ . All the snapshots correspond to the relaxed state of evolution.

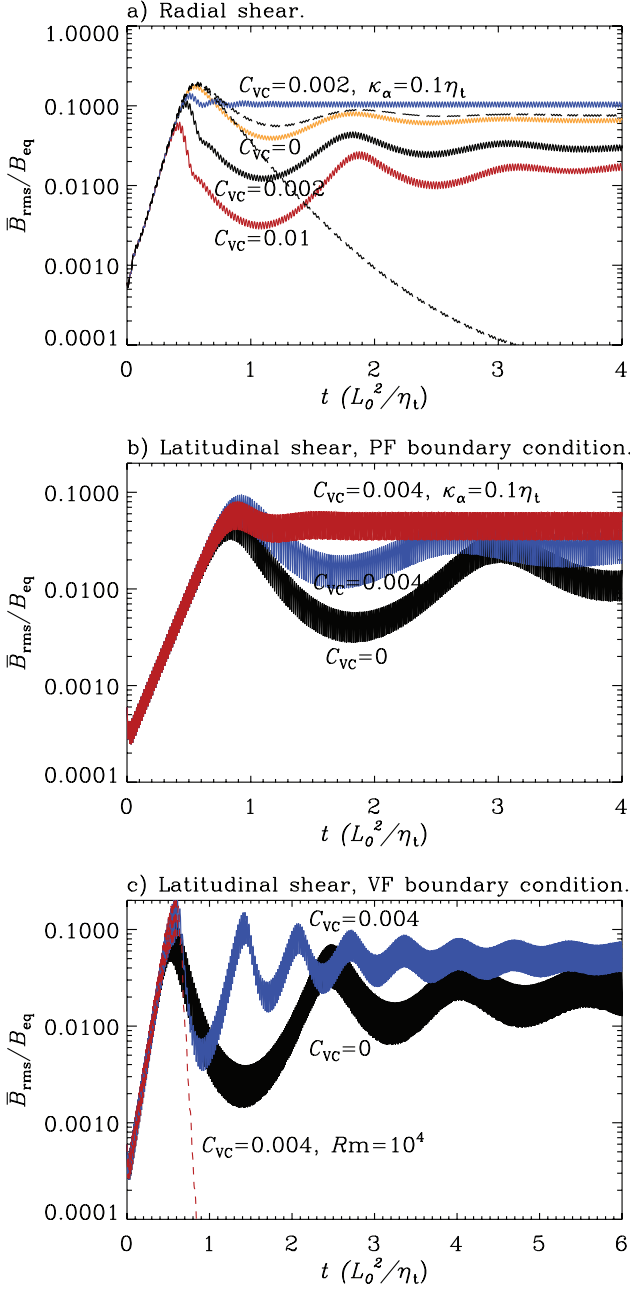


**Figure 11.** Time evolution of the averaged mean magnetic field for different values of  $C_{VC}$  and: (a) Radial shear, (b) latitudinal shear with potential field boundary conditions and (c) latitudinal shear with vertical field boundary conditions. The width of the different bands reflects the range over which the magnetic field varies during one cycle. Note that the cycle period is short compared with the resistive time-scale on which the magnetic field reaches its final saturation. If not indicated, in all models  $R_m = 10^3$ . The two dashed lines in panel (a) corresponds to  $C_{VC} = -0.002$  for  $R_m = 10^3$  and  $R_m = 10^4$ .

flux can travel either towards the bottom or the top of the dynamo region, from where magnetic helicity can be expelled. For testing this possibility, we turn off the radial shear profile and consider a purely latitudinal solar-like differential rotation:

$$\Omega(\theta) = C_\Omega \left( \frac{\eta_t}{\Omega_{\text{eq}} L_0^2} \right) [\Omega_s(\theta) - \Omega_c], \quad (17)$$

where  $\Omega_{\text{eq}}/2\pi = 460.7$  nHz is the angular velocity at the equator, and  $\Omega_s(\theta) = \Omega_{\text{eq}} + a_2 \cos^2 \theta + a_4 \cos^4 \theta$  gives the latitudinal profile,

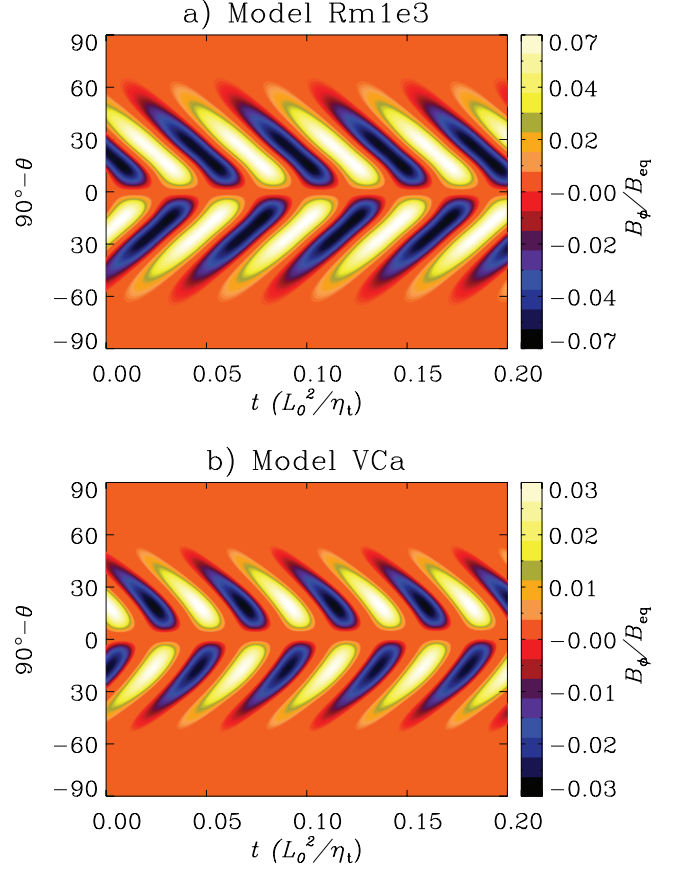


**Figure 12.** Butterfly diagrams of toroidal field for runs without the magnetic helicity flux (a) and with the VC flux (b) for  $R_m = 10^3$ . Note the stronger concentration of magnetic field at lower latitudes in the presence of the VC flux.

with  $a_2/2\pi = -62.9$  nHz and  $a_4/2\pi = -67.13$  nHz. We then multiply  $\Omega$  by a function  $\Theta(r, r_2, w_1)$  in order to confine the shear to our dynamo region.

In order for the dynamo to be slightly supercritical, as in the previous cases, we consider  $C_\Omega = 5 \times 10^4$ . This dynamo solution corresponds now to a dynamo wave produced at mid-latitudes ( $\sim 45^\circ$ ) that travels radially upwards (since  $C_\Omega$  now is positive). As in the previous cases with radial shear, the distribution of  $\nabla \cdot \mathcal{F}_{VC}/B_{\text{eq}}^2$  is similar to that of the radial derivative of magnetic energy density (left-hand panels of Figs 10b–d). If no fluxes are considered, the final amplitude of the mean magnetic field is  $\sim 0.03$  per cent of the equipartition value. In presence of VC flux, starting with  $C_{VC} = 10^{-3}$  for a model with  $R_m = 10^3$ , we notice that the final magnetic field is twice as large as in the case with  $C_{VC} = 0$ .

Our model becomes numerically unstable beyond  $C_{VC} = 10^{-2}$  due to the appearance of concentrated regions of strong  $\alpha_M$ . When VC and diffusive fluxes are considered simultaneously, with  $C_{VC} = 4 \times 10^{-3}$  and  $\kappa_\alpha = 0.1\eta_t$ , the relaxed value of  $\bar{B}_{\text{rms}}$  is only slightly below the value reached at the end of the kinematic phase (Fig. 11b). In this case  $\alpha_M$  spreads out in the convection zone, as shown in Fig. 10c, indicating that the effects of the VC flux are not important when compared with the diffusive flux.

We repeated the calculation by considering the vertical field (VF) boundary condition,  $\partial(rB_\theta)/\partial\theta = 0$ , for the top boundary, instead of the potential field (PF) condition used throughout the rest of this work. Furthermore, in the models with VF conditions the presence

of the VC flux leads to an increase of the saturated value of  $B_{\text{rms}}$  by a factor of  $\sim 2$  compared to the case without VC flux (see Fig. 11c). It may be noted that  $\alpha_M$  shows regions of both positive and negative signs in each hemisphere (see Fig. 10d). Thus, the total  $\alpha$  effect is increased locally to values well above the kinetic one. This implies that in the region around  $\pm 45^\circ$  the dynamo action is driven by the magnetic  $\alpha$  effect. A similar secondary dynamo is found to be working for a different distribution of shear and  $\alpha_K$  (Chatterjee et al. 2010b). As with PF boundary condition, large values of  $C_{\text{VC}}$  result in a numerical instability of the magnetic field in the simulation with VF.

The main result of this section is that the VC flux does not alleviate catastrophic quenching of the dynamo for large values of  $R_m$  (see the dashed lines in Figs 11a and c). The reason for this may be related to the fact that the radial flux has constituents that are either proportional to  $B_\theta$  or to  $B_\phi$  (equation 9). As  $B_\phi$  vanishes on the top boundary, and  $B_\theta$  is small, the VC flux is not able to dispose of  $\alpha_M$  across the boundary. This might change if diffusive fluxes became important near the top or if a different boundary condition on  $B$  were applied.

It should also be noted that the theoretical foundations of the VC flux have been called into question (Hubbard & Brandenburg 2010b). The criticism is connected with the fact that a shear produces spurious divergences of magnetic helicity flux that can only be removed in a gauge where the scalar potential is equal to the dot product of velocity and vector potential. In that gauge, magnetic helicity evolves merely like a passive scalar. Numerical experiments confirm that, within error bars, there is no magnetic helicity flux in situations where the formula for the VC flux would have predicted one (Hubbard & Brandenburg 2010b).

## 5 CONCLUSIONS

We have developed  $\alpha\Omega$  dynamo models in spherical geometry with relatively simple profiles of  $\alpha_K$  and shear ( $\partial\Omega/\partial r$  and  $\partial\Omega/\partial\theta$ ). We choose potential field (in some cases vertical field) and perfect conductor boundary conditions for the top and bottom boundaries, respectively. We find the critical dynamo number by fixing  $C_\Omega = -10^4$  and varying  $C_\alpha$  while using algebraic quenching.

Using a dynamo number,  $C_\Omega C_\alpha$ , that is slightly supercritical, we solve the induction equations for  $B$  and  $A$  together with an equation for the dynamical evolution of the magnetic  $\alpha$  effect,  $\alpha_M$ . We find that for positive (negative) values of  $C_\alpha$  in the Northern (Southern) hemisphere,  $\alpha_M$  is mainly negative (positive), with narrow fractions of opposite sign in regions where  $\alpha_K$  or  $\bar{B}$  are equal to zero.

The kinematic phase is, of course, independent of  $R_m$ . However, for  $R_m > 10^2$  there exists a phase of post-saturation relaxation in which the averaged magnetic field oscillates about a certain mean. The larger the  $R_m$ , the more pronounced are the damped oscillations and the longer is the relaxation time (Fig. 4). The final value of the magnetic energy obeys an  $R_m^{-1}$  dependency ( $R_m^{-0.5}$  for magnetic field modulus, Fig. 7), which is in agreement with earlier work in Cartesian coordinates (Brandenburg & Subramanian 2005b; Brandenburg et al. 2009).

We argue that including equation (6) in MFD models is appropriate for describing the saturation of the magnetic field in the dynamo process. Since we observe large-scale magnetic fields at high magnetic Reynolds numbers in astrophysical objects, there must exist a mechanism to prevent the mean magnetic field from catastrophic quenching.

We have studied the role that diffusive and VC helicity fluxes may play in this sense. Their contribution may be summarized as follows.

(i) In the presence of diffusive fluxes,  $\alpha_M$  has only one sign in each hemisphere (negative in the Northern hemisphere and positive in Southern) and is evenly distributed across the dynamo region (Fig. 9).

(ii) For  $R_m < 10^2$  the mean values of  $\alpha_M$  are similar to models without diffusive fluxes, whereas for  $R_m \geq 10^2$ ,  $\alpha_M$  has smaller values that seem to be independent of  $R_m$  (see Fig. 7, middle).

(iii) Even a very low diffusion coefficient, e.g.  $\kappa_\alpha = 0.001\eta_t$ , causes  $\bar{B}_{\text{rms}}$  to depart from the  $R_m^{-0.5}$  tendency and to converge to a constant value which is then around 5 per cent of the equipartition value for large values of  $R_m$ , up to  $R_m = 10^7$  which is the largest value used in this study (dashed line in Fig. 7, top).

(iv) Larger values of  $\kappa_\alpha$  result in larger final field strengths.

(v) In models with only radial shear the Vishniac–Cho flux contributes to  $\alpha_M$  with a component that travels in the same direction as the dynamo wave. This produces a different radial and latitudinal distribution of the magnetic  $\alpha$  effect that also affects the distribution of the magnetic fields. However, it does not help in alleviating the strong quenching at high  $R_m$ . On the contrary, the larger the coefficient  $C_{\text{VC}}$ , the smaller is the resultant magnetic field.

(vi) In models with only latitudinal shear the VC flux goes radially outward but it remains concentrated at the centre of the dynamo region. In a given hemisphere the resultant distribution of  $\alpha_M$  has both positive and negative signs. The part of  $\alpha_M$  that has the same sign as  $\alpha_K$  enhances dynamo action. This effect is more evident in models with vertical field boundary conditions (Figs 10b–d).

(vii) In models with vacuum and vertical field boundary conditions and  $R_m = 10^3$ , the VC flux increases the final value of the magnetic field by a factor of 2 compared to the case without any fluxes.

(viii) The magnetic field in models with  $R_m \geq 10^4$  and with non-zero VC flux decays after the kinematic phase since the total  $\alpha$  effect becomes subcritical (see dashed lines in Figs 11a and c). This is the result of the long decay time (long memory) for  $\alpha_M$ , which makes the dynamo recover only after several turbulent diffusion time units.

(ix) Larger values of  $C_{\text{VC}}$  produce narrow bands of  $\alpha_M$  which drives intense dynamo action in these regions. This positive feedback between the magnetic field and  $\alpha_M$  causes the simulation to become numerically unstable in the absence of any other quenching effect.

From the above results it is clear that diffusive helicity fluxes are much more important in alleviating catastrophic quenching when compared to the VC fluxes (in the form of equation 8) for a large range of  $R_m$ . This is somehow intriguing since it is known from DNS that shear in domains with open boundaries does indeed help in alleviating the catastrophic quenching. It may be understood as a result of the large value of  $C_\Omega$  compared with  $C_\alpha$  and also to the top boundary condition for the azimuthal magnetic field (Brandenburg 2005; Käpylä et al. 2008).

The results presented above indicate that considerable work is still necessary in order to understand the role of larger-scale shear in transporting and shedding small-scale magnetic helicity from the domain. Furthermore, the significance of the bump and the relaxation oscillations in models without magnetic helicity flux (Fig. 4) need to be understood. The current results may suggest that the first peak could already be sufficient to explain the strength of the large-scale magnetic field in stars and galaxies. However, the mean-field models overlook the fact that there may be several modes all

belonging to a large-scale field. It is therefore possible that one really has to wait until the end of the long relaxation period before a clear large-scale field pattern can be discerned.

In snapshots of the meridional plane as well as in butterfly diagrams, we notice that the diffusive fluxes do not significantly modify the morphology and the distribution of the magnetic field when compared with cases without fluxes or even with simulations with algebraic  $\alpha$  quenching. On the other hand, for models with VC flux the distribution of  $\alpha_M$  becomes different and so does the magnetic field. This is clear from the butterfly diagram shown in Fig. 12b, which exhibits a magnetic field confined to equatorial latitudes reminiscent of the observed butterfly diagram of the solar cycle. Even though this result corresponds to a simplified model, it illustrates the importance of considering the dynamical  $\alpha$  quenching mechanism for modelling the solar dynamo. Similar changes in the distribution of  $\alpha_M$  and  $\mathbf{B}$  are expected to happen when advection terms (meridional circulation or a stellar wind) are included in the governing equations.

In the simulations presented here,  $\Omega$  and  $\alpha$  effects are present in the same layer in each case. An interesting question is whether the quenching of the dynamo is catastrophic when both layers are segregated, as in the Parker's interface dynamo or the flux-transport dynamo models. We address this question in detail in two companion papers (Chatterjee et al. 2010a,b).

We should notice that the back-reaction of the magnetic field affects not only the  $\alpha$  effect, but also the other dynamo coefficients, including the turbulent diffusivity. Contrary to the quenching of  $\alpha$ , the quenching of  $\eta_t$  may be considered through an algebraic quenching function (see e.g. Yousef et al. 2003; Käpylä & Brandenburg 2009). Guerrero et al. (2009) have shown that in a flux-transport model these effects could change the outcome of the models such as the final magnetic field strength and its distribution in radius and latitude. Solar-like profiles of differential rotation and meridional circulation along with dynamical  $\alpha$  quenching will be considered in a forthcoming paper.

## ACKNOWLEDGMENTS

We thank Eric Blackman and Matthias Rheinhardt for their valuable comments and suggestions that have enriched and improved the contents of the manuscript. This work started during the NORDITA program on solar and stellar dynamos and cycles and is supported by the European Research Council under the AstroDyn research project 227952.

## REFERENCES

Berger M. A., Ruzmaikin A., 2000, *J. Geophys. Res.*, 105, 10481  
Blackman E. G., Brandenburg A., 2002, *ApJ*, 579, 359

Blackman E. G., Brandenburg A., 2003, *ApJ*, 584, L99  
Brandenburg A., 2001, *ApJ*, 550, 824  
Brandenburg A., 2005, *ApJ*, 625, 539  
Brandenburg A., Subramanian K., 2005a, *Phys. Rep.*, 417, 1  
Brandenburg A., Subramanian K., 2005b, *Astron. Nachr.*, 326, 400  
Brandenburg A., Dobler W., Subramanian K., 2002, *Astron. Nachr.*, 323, 99  
Brandenburg A., Käpylä P. J., Mitra D., Moss D., Tavakol R., 2007, *Astron. Nachr.*, 328, 1118  
Brandenburg A., Candelaresi S., Chatterjee P., 2009, *MNRAS*, 398, 1414  
Brown B. P., Browning M. K., Brun A. S., Miesch M. S., Toomre J., 2010, *ApJ*, 711, 424  
Charbonneau P., MacGregor K. B., 1997, *ApJ*, 486, 502  
Chatterjee P., Nandy D., Choudhuri A. R., 2004, *A&A*, 427, 1019  
Chatterjee P., Brandenburg A., Guerrero G., 2010a, *Geophys. Astrophys. Fluid Dyn.*, submitted (arXiv:1005.5708)  
Chatterjee P., Guerrero G., Brandenburg A., 2010b, *A&A*, submitted (arXiv:1005.5335)  
Dikpati M., Charbonneau P., 1999, *ApJ*, 256, 523  
Dikpati M., Choudhuri A. R., 1994, *A&A*, 291, 975  
Guerrero G., de Gouveia Dal Pino E. M., 2007, *A&A*, 464, 341  
Guerrero G., de Gouveia Dal Pino E. M., 2008, *A&A*, 485, 267  
Guerrero G., de Gouveia Dal Pino E. M., 2009, *ApJ*, 701, 725  
Hubbard A., Brandenburg A., 2010a, *Geophys. Astrophys. Fluid Dyn.*, in press (arXiv:1004.4591)  
Hubbard A., Brandenburg A., 2010b, *Astrophys. J.*, submitted (arXiv:1006.3549)  
Käpylä P. J., Brandenburg A., 2009, *ApJ*, 699, 1059  
Käpylä P. J., Korpi M. J., Brandenburg A., 2008, *A&A*, 491, 353  
Käpylä P. J., Korpi M. J., Brandenburg A., Mitra D., Tavakol R., 2010, *Astron. Nachr.*, 331, 73  
Kleeorin N., Rogachevskii I., 1999, *Phys. Rev. E*, 59, 6724  
MacGregor K. B., Charbonneau P., 1997, *ApJ*, 486, 484  
Mitra D., Candelaresi S., Chatterjee P., Tavakol R., Brandenburg A., 2010a, *Astron. Nachr.*, 331, 130  
Mitra D., Tavakol R., Käpylä P., Brandenburg A., 2010b, *ApJ*, 719, L1  
Parker E. N., 1955, *ApJ*, 122, 293  
Peaceman D. W., Rachford H. H., 1955, *J. Soc. Ind. App. Math.*, 3, 28  
Pouquet A., Frisch U., Léorat J., 1976, *J. Fluid Mech.*, 77, 321  
Shukurov A., Sokoloff D., Subramanian K., Brandenburg A., 2006, *A&A*, 448, L33  
Stix M., 1972, *A&A*, 20, 9  
Subramanian K., Brandenburg A., 2004, *Phys. Rev. Lett.*, 93, 205001  
Subramanian K., Brandenburg A., 2006, *ApJ*, 648, L71  
Sur S., Shukurov A., Subramanian K., 2007, *MNRAS*, 377, 874  
Vishniac E. T., Cho J., 2001, *ApJ*, 550, 752  
Yoshimura H., *ApJ*, 201, 740  
Yousef T. A., Brandenburg A., Rüdiger G., 2003, *A&A*, 411, 321  
Zhang H., Sokoloff D., Rogachevskii I. et al., 2006, *MNRAS*, 365, 276

This paper has been typeset from a  $\text{\TeX}/\text{\LaTeX}$  file prepared by the author.